Research Square

Preprints are preliminary reports that have not undergone peer review.
They should not be considered conclusive, used to inform clinical practice,
or referenced by the media as validated information.

GMI-Mediated Reversal of Therapeutic Resistance in Non-Small Cell Lung Cancer Through BCAT1 Downregulation and Metabolic Reprogramming

Ya-Chu Hsieh
Chung Shan Medical University
Yu-Fan Liu
Chung Shan Medical University Hospital
I-Lun Hsin
Chung Shan Medical University
Jiunn-Liang Ko
jlko@csmu.edu.tw

Chung Shan Medical University

Research Article

Keywords: EGFR tyrosine kinase inhibitor resistance, BCAT1, non–small cell lung cancer, STAT3 signaling, metabolic reprogramming, Ganoderma microsporum immunomodulatory protein (GMI)

Posted Date: November 25th, 2026

DOI: https://doi.org/10.21203/rs.3.rs-11696621/v1

License: This work is licensed under a Creative Commons Attribution 4.0 International License.
Read Full License

Additional Declarations: No competing interests reported.

GMI-Mediated Reversal of Therapeutic Resistance in Non-Small Cell Lung Cancer Through BCAT1 Downregulation and Metabolic Reprogramming

Ya-Chu Hsieh[1]; Yu-Fan Liu[2,3]* I-Lun Hsin[1]*; Jiunn-Liang Ko[1,2]*

[1] Institute of Medicine, Chung Shan Medical University, Taichung 402, Taiwan

[2] Department of Biomedical Sciences, Chung Shan Medical University, Taichung, Taiwan

[3] Division of Allergy, Department of Pediatrics, Chung Shan Medical University Hospital, Taichung, Taiwan

*Correspondence should be addressed to I-Lun Hsin (zontetsuken@gmail.com) Institute of Medicine, Chung Shan Medical University, 110, Sec. 1, Chien-Kuo N. Road, Taichung, Taiwan 40201. Tel.: +886-4-24730022 ext. 11694; Jiunn-Liang Ko (jlko@csmu.edu.tw) or Yu-Fan Liu (yfliu@csmu.edu.tw).

Abstract

Epidermal growth factor receptor tyrosine kinase inhibitors (EGFR-TKIs) have markedly improved treatment outcomes for patients with non–small cell lung cancer (NSCLC); however, the emergence of acquired resistance remains a major clinical challenge. Although resistance mechanisms have been extensively studied, the adaptive responses of cancer cells under cytotoxic drug pressure are not fully understood. In this study, we investigated the molecular and metabolic features of TKI-resistant NSCLC and evaluated a potential strategy for overcoming resistance.

We used next-generation sequencing and metabolomic analyses to characterize gefitinib- and osimertinib-resistant NSCLC cell models. Compared with TKI-sensitive cells, resistant cells exhibited significantly elevated expression of branched-chain amino acid transaminase 1 (BCAT1) and increased levels of phosphorylated STAT3. STAT3 overexpression in H1975 and HCC827 cells markedly increased BCAT1 expression and enhanced cancer cell survival. Moreover, BCAT1 overexpression promoted lung cancer cell proliferation and reduced cellular sensitivity to GMI, an immunomodulatory protein derived from Ganoderma microsporum.

Mechanistically, elevated BCAT1 expression reprogrammed branched-chain amino acid metabolism and increased α-ketoglutarate production, thereby facilitating tumor progression. Notably, GMI exerted significant antitumor activity against BCAT1-high TKI-resistant lung cancer cells in both cell-based and animal models.

In conclusion, our findings identify BCAT1 as a key metabolic regulator downstream of STAT3 in EGFR-TKI resistance and demonstrate, for the first time, that GMI suppresses gefitinib- and osimertinib-resistant NSCLC by modulating the STAT3–BCAT1 signaling axis. These results suggest that targeting BCAT1-associated metabolic reprogramming may represent a promising strategy for overcoming EGFR-TKI resistance in NSCLC.

Keywords:

EGFR tyrosine kinase inhibitor resistance; BCAT1; non–small cell lung cancer; STAT3 signaling; metabolic reprogramming; Ganoderma microsporum immunomodulatory protein (GMI)

Introduction

Tyrosine kinase inhibitors (TKIs) are a cornerstone of targeted therapy for patients with epidermal growth factor receptor (EGFR)-mutated non-small cell lung cancer (NSCLC). Osimertinib, a third-generation EGFR TKI, is widely recommended as a first-line treatment for this patient population. Other EGFR TKIs, including first-generation agents such as erlotinib and gefitinib and second-generation agents such as afatinib and dacomitinib, are also established treatment options in clinical practice [1]。 However, the development of acquired resistance remains a major obstacle that limits the long-term efficacy of molecularly targeted therapies in NSCLC [2, 3]，While drug-sensitive tumor cells typically undergo substantial apoptosis upon initial exposure to EGFR TKIs, resulting in marked tumor regression, a subset of surviving cells may acquire resistance through diverse genetic and nongenetic mechanisms[4, 5]。

Recent studies have revealed that dysregulation of branched-chain amino acid (BCAA) metabolism is associated with several human malignancies, including leukemia, breast cancer, and NSCLC [6-9]。Notably, cytosolic branched-chain amino acid aminotransferase 1 (BCAT1), which catalyzes the first step in BCAA catabolism, has emerged as a key contributor to cancer progression [10]。Increasing evidence also implicates BCAT1 in the development of therapeutic resistance in multiple tumor types [11-13]。

Bioactive compounds of plant and fungal origin have been extensively investigated for their immunomodulatory effects, health benefits, and potential therapeutic applications in cancer [14-16]. GMI, a fungal immunomodulatory protein (FIP) isolated from Ganoderma microsporum [17], has demonstrated significant antitumor activity in NSCLC, oral cancer, and melanoma [18-21] In addition, GMI has been shown to overcome drug resistance and attenuate adverse effects associated with chemotherapeutic agents such as 5-fluorouracil (5-FU) and docetaxel [22-26] , highlighting its therapeutic potential in cancer treatment.

However, whether GMI modulates BCAT1-mediated metabolic pathways and thereby influences resistance to EGFR TKIs remains unclear. In this study, we demonstrate that metabolic reprogramming plays a critical role in the development of TKI resistance in lung cancer cells and identify BCAT1 as a key mediator of this process. Furthermore, our findings suggest that GMI suppresses BCAT1 expression through modulation of STAT3 signaling, thereby attenuating resistance-associated phenotypes. Taken together, our findings reveal a previously unrecognized mechanism contributing to TKI resistance and highlight GMI as a potential therapeutic strategy for overcoming drug resistance in EGFR-mutant NSCLC.

2. Materials and Methods

2.1. Chemicals

GMI™ (manufactured by Mycomagic Biotechnology Co., Ltd., Taipei, Taiwan) was derived from Ganoderma microsporum and subsequently ameliorated. The product was stored at −20 °C until use.

2.2. Cell lines

The NSCLC cell lines H1975 (L858R/T790M) and HCC827 (exon 19 deletion), along with their drug-resistant variants HCC827/GR (gefitinib-resistant) and H1975/TR (osimertinib-resistant), were kindly provided by Dr. Ching-Chow Chen (National Taiwan University, Taiwan). Drug-resistant cells were cultured in the presence of low concentrations of gefitinib or osimertinib, respectively. All cells were maintained in RPMI-1640 medium (Gibco) supplemented with 10% fetal bovine serum (FBS), 1% penicillin–streptomycin, and 2 mM L-glutamine (Sigma-Aldrich) at 37 °C in a humidified atmosphere containing 5% CO_2.

2.3. Next-Generation Sequencing (NGS)

Total RNA was extracted 24 h after HCC827, HCC827/GR, H1975, and H1975/TR cells were treated with 0 or 12 μM GMI. RNA concentration and purity were measured using a NanoDrop ND-1000 spectrophotometer (Thermo Scientific, USA), whereas RNA integrity was assessed using an Agilent 2100 Bioanalyzer with an RNA 6000 Nano Kit. RNA-seq libraries were prepared using the SureSelect XT HS2 mRNA Library Prep Kit (Agilent, USA), with size selection performed using AMPure XP beads (Beckman Coulter, USA) according to the manufacturer's protocols. Sequencing was conducted on an Illumina platform using sequencing-by-synthesis (SBS) technology. FASTQ files were generated by Welgene Biotech using BCL Convert v4.2.4.

2.4. Metabolomic Analysis

Metabolomic profiling was performed using the NSCLC cell line H1975 and its drug-resistant derivative H1975/TR. Cells were treated with 0 or 12 μM GMI for 24 h, after which samples were collected for subsequent metabolomic analysis. Metabolite analysis was performed using UHPLC-MS/MS with electrospray ionization (ESI) in both positive and negative ion modes to maximize metabolite coverage. MS1 data were processed using the xcms package (v3.12.0) in R for peak detection and grouping [11, 12], with parameter optimization performed via the Autotuner package (v1.4.0). Data-dependent acquisition (DDA)-based MS2 spectra were used to support metabolite identification. After data preprocessing and normalization, both univariate and

multivariate statistical analyses were performed. Multivariate analyses, including PCA and OPLS-DA, were used to assess sample clustering and variability. Differential metabolites were identified using Student's t-test ($p < 0.05$) and fold-change criteria and visualized using volcano plots.

2.5. Western Blot Analysis

Cells were lysed in RIPA buffer supplemented with phosphatase and protease inhibitors. Protein concentrations were determined using the Bio-Rad Protein Assay Kit, and equal amounts of protein were separated by 10% SDS–PAGE and transferred to PVDF membranes. After overnight incubation with primary antibodies at 4 °C and incubation with secondary antibodies for 2 h at room temperature, protein bands were detected using the Bio-Rad ChemiDoc MP system.

2.6. Antibodies

HA-tag (#3724) were purchased from Cell Signaling Technology (Boston, MA, USA). BCAT1 (A16351) and alpha-Tubulin (A6830), were purchased from ABclonal (USA, MA). β-actin (Sigma, AC-40)

2.7. Colony Formation Assay

To evaluate long-term proliferative capacity, lung cancer cells were treated with GMI (0 or 2.4 μM) for 24 h, harvested, and seeded into 6-well plates at a density of 400 cells per well. After 10–14 days of incubation, colonies were fixed with 95% ethanol for 15 min, stained with 20% Giemsa solution for 20 min, and washed with distilled water. Colonies containing more than 50 cells were counted under a light microscope. Assays were performed in triplicate, and colony formation was expressed as a percentage of the untreated control.

2.8. MTT Assay

Cell viability was determined using the MTT assay. NSCLC cells were seeded in 96-well plates (8×10^3 cells/well) and treated with GMI (0, 0.3, 0.6, 1.2, or 2.4 μM) for 24 or 48 h. MTT solution (5 mg/mL, 20 μL/well) was then added, followed by incubation at 37 °C for 4 h. The resulting formazan crystals were dissolved in 100 μL of dimethyl sulfoxide (DMSO), and absorbance was measured at 570 nm. Cell viability was calculated relative to the untreated control. All experiments were performed in triplicate.

2.9. In vivo xenograft model and drug administration

HCC827/GR cells (5×10^6 cells suspended in 100 μL of a Matrigel/PBS mixture, 1:1, v/v) were subcutaneously injected into the right dorsal flank of 5-week-old BALB/c nude mice. When tumors reached approximately 50 mm^3, mice were randomly assigned

to control or GMI-treated groups and received daily oral gavage of PBS (100 μL) or GMI (80 μg in 100 μL PBS), respectively. Tumor dimensions were measured using calipers, and tumor volume was calculated as $TV = (L \times W^2)/2$, where L and W represent the longest and shortest tumor diameters, respectively. All animal experiments were approved by the Institutional Animal Care and Use Committee of Chung Shan Medical University (IACUC approval no. 2608).

2.10. Metabolite detection assays

Intracellular levels of α-ketoglutarate (α-KG), glutamate, and reduced and oxidized glutathione (GSH and GSSG) were measured using commercial assay kits (Elabscience, E-BC-F047; Abcam, ab83389 and ab239709, respectively) according to the manufacturers' instructions. Absorbance was measured using a microplate reader, and metabolite levels were calculated and normalized to the cell number.

2.11. Quantitative Reverse Transcription PCR

Total RNA was isolated from cultured cells using the Rare-RNA kit (GenePure Technology, Taiwan), and cDNA was synthesized using the High-Capacity cDNA Reverse Transcription Kit (Applied Biosystems). Quantitative reverse transcription PCR (qRT-PCR) was performed using SYBR Green reagent (Protech). Target gene expression was normalized to β-actin mRNA levels.

2.12. Graphical Abstract

The graphical abstract was generated using FigureLabs (https://chat.figurelabs.ai/) and subsequently reviewed and revised by the authors to ensure scientific accuracy and consistency with the findings of this study.

2.13. Statistical analysis

Data are presented as means ± standard deviations (SDs) from three independent experiments. Statistical analyses were performed using SPSS version 18 (IBM Corp., Armonk, NY, USA) and GraphPad Prism 10 (GraphPad Software, San Diego, CA, USA). Differences between two groups were evaluated using Student's t-test. A p value < 0.05 was considered statistically significant.

3. Results

3.1 BCAT1-associated transcriptomic alterations in drug-resistant lung cancer cells

To investigate the association between differential BCAT1 expression and transcriptomic alterations in lung cancer cells, RNA sequencing (RNA-seq) was performed using H1975, H1975/TR, HCC827, and HCC827/GR cell lines. Differential expression analysis revealed that, compared with their respective parental counterparts, drug-resistant cells shared 119 upregulated genes. In addition, 789 and 1,349 genes were uniquely upregulated in HCC827/GR and H1975/TR cells, respectively (Figure 1A). In contrast, analysis of downregulated genes identified 200 genes that were downregulated in both resistant cell lines, along with 869 genes uniquely downregulated in HCC827/GR cells and 1,754 genes uniquely downregulated in H1975/TR cells (Figure 1B).

Gene Ontology (GO) enrichment analysis demonstrated that the differentially expressed genes were significantly enriched in biological processes related to amino acid metabolism, redox homeostasis, energy production, and mitochondria-associated metabolic pathways. Notably, pathways associated with branched-chain amino acid (BCAA) metabolism and α-ketoglutarate (α-KG) metabolism were prominently represented (Figure 1C).

Volcano plot analysis further revealed distinct transcriptomic differences between parental and drug-resistant cell lines. Multiple metabolism-related genes exhibited increased expression in drug-resistant cells, including BCAT1 and related metabolic genes, which were expressed at higher levels in H1975/TR and HCC827/GR cells than in their respective parental cells (Figure 1D).

Further analysis showed that, BCAT1 expression was markedly reduced in drug-resistant cells following GMI treatment, accompanied by coordinated downregulation of genes involved in amino acid transport and metabolism (Figure 1E). Based on these observations, a schematic model was generated to illustrate the potential role of BCAT1 in BCAA catabolism, α-KG conversion, and glutamate production (Figure 1F).

3.2 Association of BCAT1 expression with drug-resistant lung cancer cell lines and clinical outcomes

BCAT1 expression was examined in parental lung cancer cell lines, gefitinib- and osimertinib-resistant sublines, and clinical datasets. Quantitative RT-PCR analysis showed that BCAT1 mRNA levels were significantly higher in HCC827/GR cells than in parental HCC827 cells and were also significantly elevated in H1975/TR cells compared with H1975 cells. In addition, treatment with GMI reduced BCAT1 mRNA expression in a dose-dependent manner in both drug-resistant cell lines (Figure 2A).

Consistent with the mRNA results, immunoblot analysis confirmed that BCAT1 protein expression was higher in H1975/TR and HCC827/GR cells than in their respective parental counterparts (Figure 2B). Further analysis demonstrated that BCAT1 protein levels in drug-resistant cells progressively decreased following GMI treatment (Figure 2C).

To assess the clinical relevance of BCAT1, we analyzed The Cancer Genome Atlas lung adenocarcinoma (TCGA-LUAD) dataset. BCAT1 expression was significantly higher in tumor tissues than in normal lung tissue samples (Figure 2D).

3.3 Effects of BCAT1 overexpression on lung cancer cells under GMI treatment

BCAT1 was stably overexpressed in H1975 and HCC827 cells, and stable BCAT1 protein overexpression was confirmed by immunoblot analysis (Figure 3A). MTT assays showed that GMI treatment markedly reduced cell viability in vector-control cells, whereas BCAT1 overexpression significantly increased cell viability following GMI treatment (Figure 3B).

Colony formation assays further demonstrated that BCAT1 overexpression partially restored clonogenic survival following GMI treatment relative to vector-control cells (Figure 3C). Quantitative analysis of colony numbers corroborated these observations (Figure 3D).

3.4. STAT3 Regulation of BCAT1 Expression and Its Impact on GMI Sensitivity

H1975 and HCC827 cells were transfected with a vector encoding HA-tagged STAT3 or an empty vector and subsequently treated with GMI. Immunoblot analysis showed that STAT3 overexpression increased BCAT1 protein levels in both cell lines. GMI treatment reduced BCAT1 expression in a dose-dependent manner; however, STAT3 overexpression attenuated the GMI-induced decrease in BCAT1 protein levels (Figure 4A).

Cell viability assays demonstrated that cells overexpressing STAT3 exhibited higher viability than empty-vector-transfected controls across all tested concentrations of GMI (Figure 4B). Quantitative PCR analysis further showed that STAT3 overexpression increased BCAT1 mRNA levels, whereas GMI treatment reduced BCAT1 mRNA expression. Notably, STAT3 overexpression partially restored BCAT1 mRNA expression in the presence of GMI (Figure 4C).

3.5. Reprogramming of Glutamate Metabolism in Drug-Resistant Lung Cancer Cells

Intracellular glutamate levels were measured in parental lung cancer cell lines (H1975 and HCC827) and their corresponding drug-resistant derivatives (H1975/TR

and HCC827/GR). Drug-resistant cells exhibited different intracellular glutamate profiles from those of parental cells following treatment with increasing concentrations of GMI. Both H1975/TR and HCC827/GR cells showed dose-dependent alterations in intracellular glutamate levels, suggesting altered glutamate metabolism associated with acquired drug resistance (Figure 5A).

Given the role of glutamate in redox regulation, intracellular reduced glutathione (GSH) levels were subsequently assessed. Drug-resistant cells exhibited different GSH levels from those of their parental counterparts, with H1975/TR cells exhibiting higher basal GSH levels. GMI treatment reduced GSH levels in a dose-dependent manner, which was particularly pronounced in HCC827 and HCC827/GR cells (Figure 5B).

Cell viability assays demonstrated that GMI treatment significantly reduced viability across all tested cell lines, although drug-resistant cells were less sensitive to GMI than their parental counterparts. Treatment with α-ketoglutarate (α-KG) alone had little effect on cell viability, while combined treatment with α-KG and GMI further increased cell viability (Figure 5C).

Colony formation assays showed that treatment with dimethyl-α-ketoglutarate (DM-αKG) alone increased colony numbers, whereas GMI markedly suppressed clonogenic growth. Notably, the combined treatment partially restored colony formation relative to GMI treatment alone (Figure 5D). Quantitative analysis of clonogenic survival confirmed these observations (Figure 5E).

3.6 GMI suppresses the growth of drug-resistant lung cancer xenografts and reduces BCAT1 expression

The in vivo antitumor effects of GMI were evaluated using an HCC827/GR xenograft model. Tumor growth was markedly suppressed in the GMI-treated group. At day 50, mean tumor volume was significantly lower in mice receiving GMI (80 μg per mouse by oral gavage; n = 4) than in control mice, and tumor volumes were lower than those in the control group throughout the treatment period (Figure 6A). Bioluminescence imaging further showed a reduced tumor burden in mice receiving GMI treatment compared with controls (Figure 6B).

At the experimental endpoint, excised tumors from the GMI-treated group were smaller, with significantly reduced tumor volumes and weights relative to the control group (Figures 6C and 6D).

Immunohistochemical analysis revealed reduced BCAT1 expression in tumors from GMI-treated mice relative to controls (Figure 6E). Quantitative analysis further confirmed that GMI treatment significantly decreased BCAT1 protein levels in xenograft tumors (Figure 6F). Immunohistochemical analysis revealed heterogeneous

BCAT1 expression across lung cancer specimens, with strong cytoplasmic staining observed in tumors with high BCAT1 expression and weak or minimal staining detected in tumors with low BCAT1 expression (Figure 6G). Kaplan–Meier survival analysis demonstrated that patients with high BCAT1 expression exhibited significantly poorer overall survival than those with low BCAT1 expression (Figure 6H).

Discussion

Acquired resistance to EGFR tyrosine kinase inhibitors (TKIs) remains a major clinical challenge in the treatment of NSCLC [27, 28]. Although diverse genetic and signaling mechanisms underlying TKI resistance have been extensively characterized, including secondary EGFR mutations and bypass pathway activation [29, 30], how cancer cells adapt their metabolic programs to survive cytotoxic drug pressure is less well understood [31]. In the present study, we demonstrate that metabolic reprogramming mediated by the STAT3–BCAT1 axis plays a pivotal role in gefitinib- and osimertinib-resistant lung cancer cells and that the immunomodulatory protein GMI suppresses this adaptive pathway in drug-resistant cells.

Using integrated transcriptomic and metabolomic analyses, we identified BCAT1 as a metabolic enzyme consistently upregulated in both gefitinib- and osimertinib-resistant NSCLC cell lines. RNA-seq analysis revealed that drug-resistant cells shared a distinct transcriptional signature enriched in pathways related to amino acid metabolism, redox regulation, and mitochondrial metabolism. Notably, pathways associated with branched-chain amino acid (BCAA) metabolism and α-ketoglutarate (α-KG) metabolism were prominently represented. These findings are consistent with accumulating evidence that metabolic plasticity is a hallmark of acquired drug resistance and tumor adaptation under therapeutic stress [32, 33].

BCAT1 catalyzes the reversible transamination of BCAAs to produce glutamate and branched-chain α-keto acids, thereby linking BCAA metabolism to the tricarboxylic acid (TCA) cycle and cellular redox homeostasis [34]. In our study, drug-resistant lung cancer cells exhibited altered intracellular glutamate and glutathione (GSH) levels, indicating changes in antioxidant capacity and metabolic flexibility. This observation is in line with previous studies demonstrating that increased glutamate and GSH production can support cancer cell survival by buffering oxidative stress and sustaining mitochondrial metabolism [35, 36]. Furthermore, the partial restoration of clonogenic growth by α-KG supplementation in GMI-treated cells supports the functional importance of BCAT1-associated metabolic pathways in cancer cell survival and proliferation.

Importantly, we demonstrate that BCAT1 expression is regulated, at least in part, by STAT3 signaling in lung cancer cells. STAT3 overexpression increased BCAT1 mRNA and protein levels and reduced sensitivity to GMI treatment. Conversely, GMI treatment suppressed BCAT1 expression even in STAT3-overexpressing cells. Persistent STAT3

activation has been widely implicated in EGFR TKI resistance, epithelial–mesenchymal transition, and poor prognosis in NSCLC[37-39]. Our findings extend these observations by identifying BCAT1 as a potential downstream effector of STAT3-driven metabolic reprogramming, thereby providing a mechanistic link between oncogenic signaling and metabolic adaptation in drug-resistant lung cancer cells.

The clinical relevance of BCAT1 was further supported by analysis of the TCGA-LUAD dataset and human lung cancer specimens. BCAT1 expression was higher in tumor tissues than in normal tissues, and high expression was associated with poorer overall survival. These findings are consistent with prior reports showing that BCAT1 overexpression is associated with aggressive tumor behavior and unfavorable prognosis in multiple malignancies, including glioblastoma, leukemia, and hepatocellular carcinoma [40]. Thus, BCAT1 may function as a mediator of metabolic adaptation and a potential prognostic biomarker in NSCLC.

A key finding of this study is the demonstration that GMI effectively suppresses BCAT1 expression and inhibits tumor growth in both cell-based and animal models of TKI-resistant lung cancer. In the HCC827/GR xenograft model, oral administration of GMI significantly reduced tumor burden and BCAT1 expression. Notably, GMI is a natural immunomodulatory protein that has been described as a dietary ingredient; however, its clinical safety and regulatory status require further verification. GMI may exert its antitumor effects in part by modulating STAT3-associated metabolic reprogramming. This mode of action may be advantageous, as it may offer an approach to targeting metabolic adaptations that accompany EGFR-TKI resistance, including resistance associated with secondary EGFR mutations such as T790M and C797S [41, 42]. Collectively, these findings support the translational relevance of GMI as a potential adjunct strategy for overcoming EGFR TKI resistance in NSCLC.

Despite these strengths, several limitations should be acknowledged. First, although our data support a role for BCAT1 in metabolic adaptation and drug resistance, the mechanisms linking STAT3 signaling to BCAT1 regulation require further clarification. Second, while our in vivo studies demonstrate antitumor efficacy of GMI, further pharmacokinetic and toxicity evaluations are necessary to assess its translational potential. Finally, whether BCAT1 inhibition acts synergistically with EGFR TKIs or other metabolic inhibitors warrants further investigation.

In conclusion, our study identifies BCAT1-mediated metabolic reprogramming as a critical adaptive mechanism in gefitinib- and osimertinib-resistant lung cancer cells and identifies GMI as a potential modulator of the STAT3–BCAT1 signaling axis. These

findings provide new insights into the metabolic basis of EGFR TKI resistance and highlight BCAT1 as a promising therapeutic target for addressing drug resistance in NSCLC.

Acknowledgments

We thank MycoMagic Biotechnology Co., Ltd. for providing GMI samples and Dr. Ching-Chow Chen (National Taiwan University) for providing the cell lines. Flow cytometry experiments were performed at the Instrument Center of Chung Shan Medical University.

Consent for publication

Not applicable. This manuscript does not contain identifiable individual-level data.

Data availability statement

The data supporting the findings of this study are available from the corresponding author upon reasonable request.

CRediT authorship contribution statement

Ya-Chu Hsieh: Investigation, Data curation, Formal analysis, Writing – original draft. Yu-Fan Liu: Supervision, Project administration. I-Lun Hsin: Investigation, Data curation, Supervision. Jiunn-Liang Ko: Writing – review and editing, Writing – original draft, Supervision, Project administration, Funding acquisition.

Declaration of competing interest

The authors declare no conflicts of interest.

Funding

This work was supported by the Taiwan National Science and Technology Council (grant number NSTC 114-2320-B-040-018-MY3).

Reference

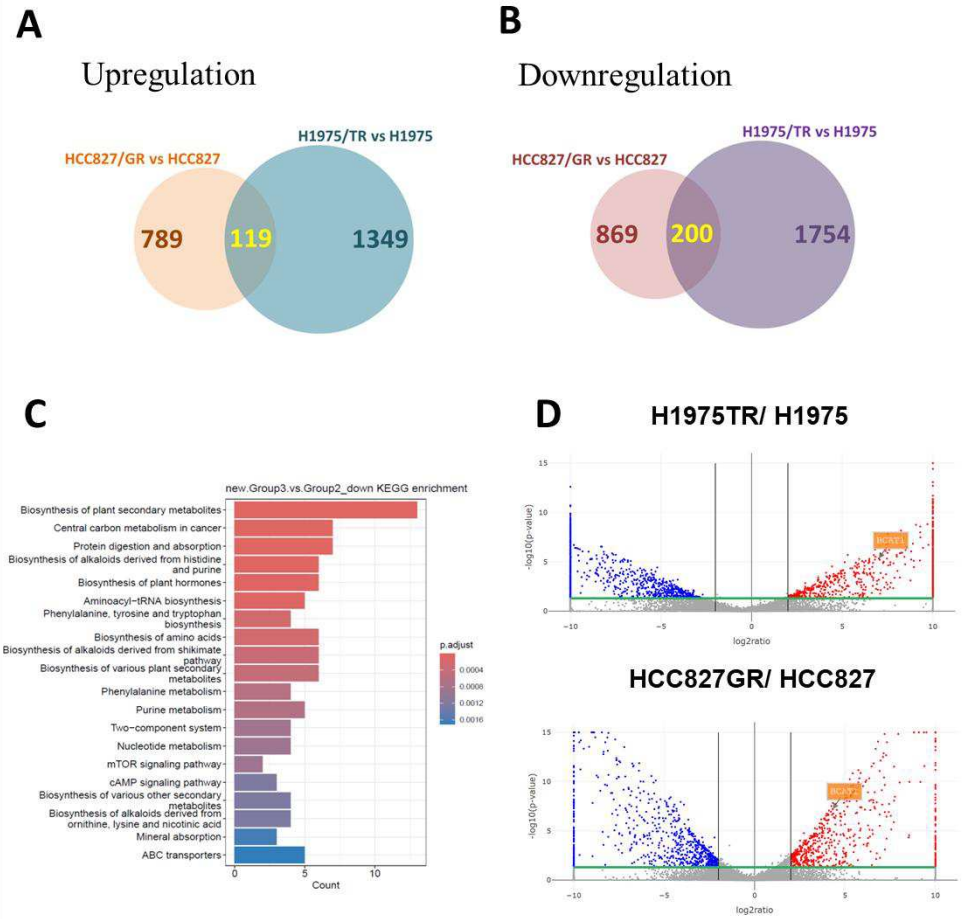
1. Johnson M, Garassino MC, Mok T, Mitsudomi T. Treatment strategies and outcomes for patients with EGFR-mutant non-small cell lung cancer resistant to EGFR tyrosine kinase inhibitors: Focus on novel therapies. Lung Cancer. 2022; 170: 41-51.
2. Lin Z, Li J, Zhang J, Feng W, Lu J, Ma X, et al. Metabolic Reprogramming Driven by IGF2BP3 Promotes Acquired Resistance to EGFR Inhibitors in Non-Small Cell Lung Cancer. Cancer Res. 2023; 83: 2187-207.
3. Wu SG, Shih JY. Management of acquired resistance to EGFR TKI-targeted therapy in advanced non-small cell lung cancer. Mol Cancer. 2018; 17: 38.
4. Hata AN, Niederst MJ, Archibald HL, Gomez-Caraballo M, Siddiqui FM, Mulvey HE, et al. Tumor cells can follow distinct evolutionary paths to become resistant to epidermal growth factor receptor inhibition. Nat Med. 2016; 22: 262-9.
5. Holohan C, Van Schaeybroeck S, Longley DB, Johnston PG. Cancer drug resistance: an evolving paradigm. Nat Rev Cancer. 2013; 13: 714-26.
6. Wang H, Wang F, Ouyang W, Jiang X, Wang Y. BCAT1 overexpression regulates proliferation and c-Myc/GLUT1 signaling in head and neck squamous cell carcinoma. Oncol Rep. 2021; 45.
7. Tosello V, Rompietti C, Papathanassiu AE, Arrigoni G, Piovan E. BCAT1 Associates with DNA Repair Proteins KU70 and KU80 and Contributes to Regulate DNA Repair in T-Cell Acute Lymphoblastic Leukemia (T-ALL). Int J Mol Sci. 2024; 25.
8. Thewes V, Simon R, Hlevnjak M, Schlotter M, Schroeter P, Schmidt K, et al. The branched-chain amino acid transaminase 1 sustains growth of antiestrogen-resistant and ERalpha-negative breast cancer. Oncogene. 2017; 36: 4124-34.
9. Zhang T, Pan Z, Gao J, Wu Q, Bai G, Li Y, et al. Branched-chain amino acid transaminase 1 confers EGFR-TKI resistance through epigenetic glycolytic activation. Signal Transduct Target Ther. 2024; 9: 216.
10. Hattori A, Tsunoda M, Konuma T, Kobayashi M, Nagy T, Glushka J, et al. Cancer progression by reprogrammed BCAA metabolism in myeloid leukaemia. Nature. 2017; 545: 500-4.
11. Jiang Y, Zhang D, He X, Chen C, Xie L, Liu L, et al. BCAT1 contributes to the development of TKI-resistant CML. Cell Oncol (Dordr). 2025; 48: 411-24.
12. Zheng YH, Hu WJ, Chen BC, Grahn TH, Zhao YR, Bao HL, et al. BCAT1, a key prognostic predictor of hepatocellular carcinoma, promotes cell proliferation and induces chemoresistance to cisplatin. Liver Int. 2016; 36: 1836-47.
13. Cho HR, Hong B, Kim H, Park CK, Park SH, Park S, et al. Assessment of bevacizumab resistance increased by expression of BCAT1 in IDH1 wild-type glioblastoma: application of DSC perfusion MR imaging. Oncotarget. 2016; 7: 69606-15.

14. Zhao S, Gao Q, Rong C, Wang S, Zhao Z, Liu Y, et al. Immunomodulatory Effects of Edible and Medicinal Mushrooms and Their Bioactive Immunoregulatory Products. J Fungi (Basel). 2020; 6.
15. Lysakowska P, Sobota A, Wirkijowska A. Medicinal Mushrooms: Their Bioactive Components, Nutritional Value and Application in Functional Food Production-A Review. Molecules. 2023; 28.
16. Abdelmoaty MM, Kadry R, Mosley RL, Gendelman HE. Neuroprotective Mushrooms. NeuroImmune Pharm Ther. 2024; 3: 129-37.
17. Ejike UC, Chan CJ, Okechukwu PN, Lim RLH. New advances and potentials of fungal immunomodulatory proteins for therapeutic purposes. Crit Rev Biotechnol. 2020; 40: 1172-90.
18. Hsin IL, Ou CC, Wu TC, Jan MS, Wu MF, Chiu LY, et al. GMI, an immunomodulatory protein from Ganoderma microsporum, induces autophagy in non-small cell lung cancer cells. Autophagy. 2011; 7: 873-82.
19. Hsin IL, Ou CC, Wu MF, Jan MS, Hsiao YM, Lin CH, et al. GMI, an Immunomodulatory Protein from Ganoderma microsporum, Potentiates Cisplatin-Induced Apoptosis via Autophagy in Lung Cancer Cells. Mol Pharm. 2015; 12: 1534-43.
20. Hsin IL, Hsu JC, Wu WJ, Lu HJ, Wu MF, Ko JL. GMI, a fungal immunomodulatory protein from Ganoderma microsporum, induce apoptosis via beta-catenin suppression in lung cancer cells. Environ Toxicol. 2018; 33: 955-61.
21. Lu CT, Leong PY, Hou TY, Kang YT, Chiang YC, Hsu CT, et al. Inhibition of proliferation and migration of melanoma cells by ketoconazole and Ganoderma immunomodulatory proteins. Oncol Lett. 2019; 18: 891-7.
22. Kang YT, Chang HY, Hsieh YC, Chou CH, Hsin IL, Ko JL. Integrin alphaV Inhibition by GMI, a Ganoderma Microsporum Immunomodulatory Protein, Abolish Stemness and Migration in EGFR-Mutated Lung Cancer Cells Resistant to Osimertinib. Environ Toxicol. 2024; 39: 5238-49.
23. Chiu LY, Hu ME, Yang TY, Hsin IL, Ko JL, Tsai KJ, et al. Immunomodulatory Protein from Ganoderma microsporum Induces Pro-Death Autophagy through Akt-mTOR-p70S6K Pathway Inhibition in Multidrug Resistant Lung Cancer Cells. PLoS One. 2015; 10: e0125774.
24. Hsin IL, Chiu LY, Ou CC, Wu WJ, Sheu GT, Ko JL. CD133 inhibition via autophagic degradation in pemetrexed-resistant lung cancer cells by GMI, a fungal immunomodulatory protein from Ganoderma microsporum. Br J Cancer. 2020; 123: 449-58.
25. Chiu LY, Hsin IL, Tsai JN, Chen CJ, Ou CC, Wu WJ, et al. Combination treatment of Src inhibitor Saracatinib with GMI, a Ganoderma microsporum immunomodulatory

protein, induce synthetic lethality via autophagy and apoptosis in lung cancer cells. J Cell Physiol. 2021; 236: 1148-57.
26. Li CH, Ko JL, Ou CC, Lin WL, Yen CC, Hsu CT, et al. The Protective Role of GMI, an Immunomodulatory Protein From Ganoderma microsporum, on 5-Fluorouracil-Induced Oral and Intestinal Mucositis. Integr Cancer Ther. 2019; 18: 1534735419833795.
27. Chen G, Feng J, Zhou C, Wu YL, Liu XQ, Wang C, et al. Quality of life (QoL) analyses from OPTIMAL (CTONG-0802), a phase III, randomised, open-label study of first-line erlotinib versus chemotherapy in patients with advanced EGFR mutation-positive non-small-cell lung cancer (NSCLC). Ann Oncol. 2013; 24: 1615-22.
28. Ramalingam SS, Vansteenkiste J, Planchard D, Cho BC, Gray JE, Ohe Y, et al. Overall Survival with Osimertinib in Untreated, EGFR-Mutated Advanced NSCLC. N Engl J Med. 2020; 382: 41-50.
29. Bean J, Brennan C, Shih JY, Riely G, Viale A, Wang L, et al. MET amplification occurs with or without T790M mutations in EGFR mutant lung tumors with acquired resistance to gefitinib or erlotinib. Proc Natl Acad Sci U S A. 2007; 104: 20932-7.
30. Engelman JA, Zejnullahu K, Mitsudomi T, Song Y, Hyland C, Park JO, et al. MET amplification leads to gefitinib resistance in lung cancer by activating ERBB3 signaling. Science. 2007; 316: 1039-43.
31. Pavlova NN, Thompson CB. The Emerging Hallmarks of Cancer Metabolism. Cell Metab. 2016; 23: 27-47.
32. Vander Heiden MG, DeBerardinis RJ. Understanding the Intersections between Metabolism and Cancer Biology. Cell. 2017; 168: 657-69.
33. Ward PS, Thompson CB. Metabolic reprogramming: a cancer hallmark even warburg did not anticipate. Cancer Cell. 2012; 21: 297-308.
34. Xiong H, Liu R, Xu K, Chen X, Huang L, Shou Y, et al. Branched-chain amino acid and cancer: metabolism, immune microenvironment and therapeutic targets. J Transl Med. 2025; 23: 636.
35. Lu SC. Glutathione synthesis. Biochim Biophys Acta. 2013; 1830: 3143-53.
36. Wang YN, Lu YX, Liu J, Jin Y, Bi HC, Zhao Q, et al. AMPKalpha1 confers survival advantage of colorectal cancer cells under metabolic stress by promoting redox balance through the regulation of glutathione reductase phosphorylation. Oncogene. 2020; 39: 637-50.
37. Sadrkhanloo M, Paskeh MDA, Hashemi M, Raesi R, Motahhary M, Saghari S, et al. STAT3 signaling in prostate cancer progression and therapy resistance: An oncogenic pathway with diverse functions. Biomed Pharmacother. 2023; 158: 114168.
38. Ao J, Fei J, Wang G, Zhang W, Yu S, Guo R, et al. pSTAT3 transactivates EGFR in

maintaining EGFR protein homeostasis and EGFR-TKI resistance. Acta Biochim Biophys Sin (Shanghai). 2024; 57: 310-6.
39. Tan FH, Putoczki TL, Stylli SS, Luwor RB. The role of STAT3 signaling in mediating tumor resistance to cancer therapy. Curr Drug Targets. 2014; 15: 1341-53.
40. Tonjes M, Barbus S, Park YJ, Wang W, Schlotter M, Lindroth AM, et al. BCAT1 promotes cell proliferation through amino acid catabolism in gliomas carrying wild-type IDH1. Nat Med. 2013; 19: 901-8.
41. Wang R, Chen Y, Li L, Zhang L, Zhang S. Osimertinib acquired resistance among patients with EGFR-mutated NSCLC: from molecular mechanisms to clinical therapeutic strategies. Cancer Drug Resist. 2025; 8: 61.
42. Leonetti A, Sharma S, Minari R, Perego P, Giovannetti E, Tiseo M. Resistance mechanisms to osimertinib in EGFR-mutated non-small cell lung cancer. Br J Cancer. 2019; 121: 725-37.

Figure legends



E

	HCC827/GR GMI 1.2 μM vs GMI 0 μM	H1975/TR GMI 1.2 μM vs GMI 0 μM
Gene name	**ratio**	**ratio**
ALDH1A1	0.53	0.66
ALPK2	0.26	0.25
ANKRD33B	0.56	0.31
AXL	0.3	0.76
BCAT1	0.64	0.32
CDH2	0.73	0.6
CHST10	0.47	0.47
CLU	0.5	0.63
COL4A1	0.8	0.63
COL4A2	0.9	0.82
COL5A1	0.65	0.35
CYFIP2	0.44	0.5
DIO2	0.05	0.14
DPYSL5	0.42	0.34
EDN1	0.23	0.65
GLIPR1	0.4	0.62
INA	0.63	0.65
KIAA1549L	0.7	0.55
MSRB3	0.62	0.65
NUAK2	0.48	0.43
PLCB4	0.31	0.52
TENM3	0.62	0.56
TPM1	0.5	0.4
TUB	0.25	0.32

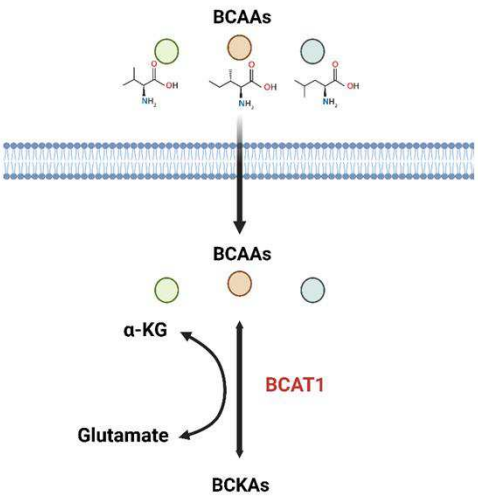


Figure 1. Identification of differentially expressed genes and metabolic pathways associated with GMI treatment in EGFR-TKI-resistant NSCLC cells.

(A) Venn diagram showing the overlap of upregulated genes identified in HCC827/GR cells compared with parental HCC827 cells and H1975/TR cells compared with parental H1975 cells. (B) Venn diagram illustrating the overlap of downregulated genes identified in the two EGFR-TKI-resistant NSCLC cell models. (C) Kyoto Encyclopedia of Genes and Genomes (KEGG) pathway enrichment analysis of downregulated genes following GMI treatment, highlighting the metabolic pathways potentially affected by GMI. (D) Volcano plots showing differentially expressed genes in H1975/TR and HCC827/GR cells relative to their respective parental cell lines. BCAT1 is highlighted as a candidate gene associated with metabolic reprogramming in EGFR-TKI-resistant NSCLC cells. Red and blue dots indicate upregulated and downregulated genes, respectively, whereas gray dots represent genes without significant differential expression. (E) Relative expression ratios of selected genes in HCC827/GR and H1975/TR cells following treatment with GMI (1.2 μM) compared with untreated controls (0 μM). BCAT1 expression was reduced in both resistant cell lines following GMI treatment. (F) Schematic illustration of BCAT1-mediated branched-chain amino acid (BCAA) metabolism. BCAT1 catalyzes the reversible transamination of BCAAs into branched-chain keto acids (BCKAs), using α-ketoglutarate (α-KG) as an amino group acceptor and generating glutamate.

Figure 2

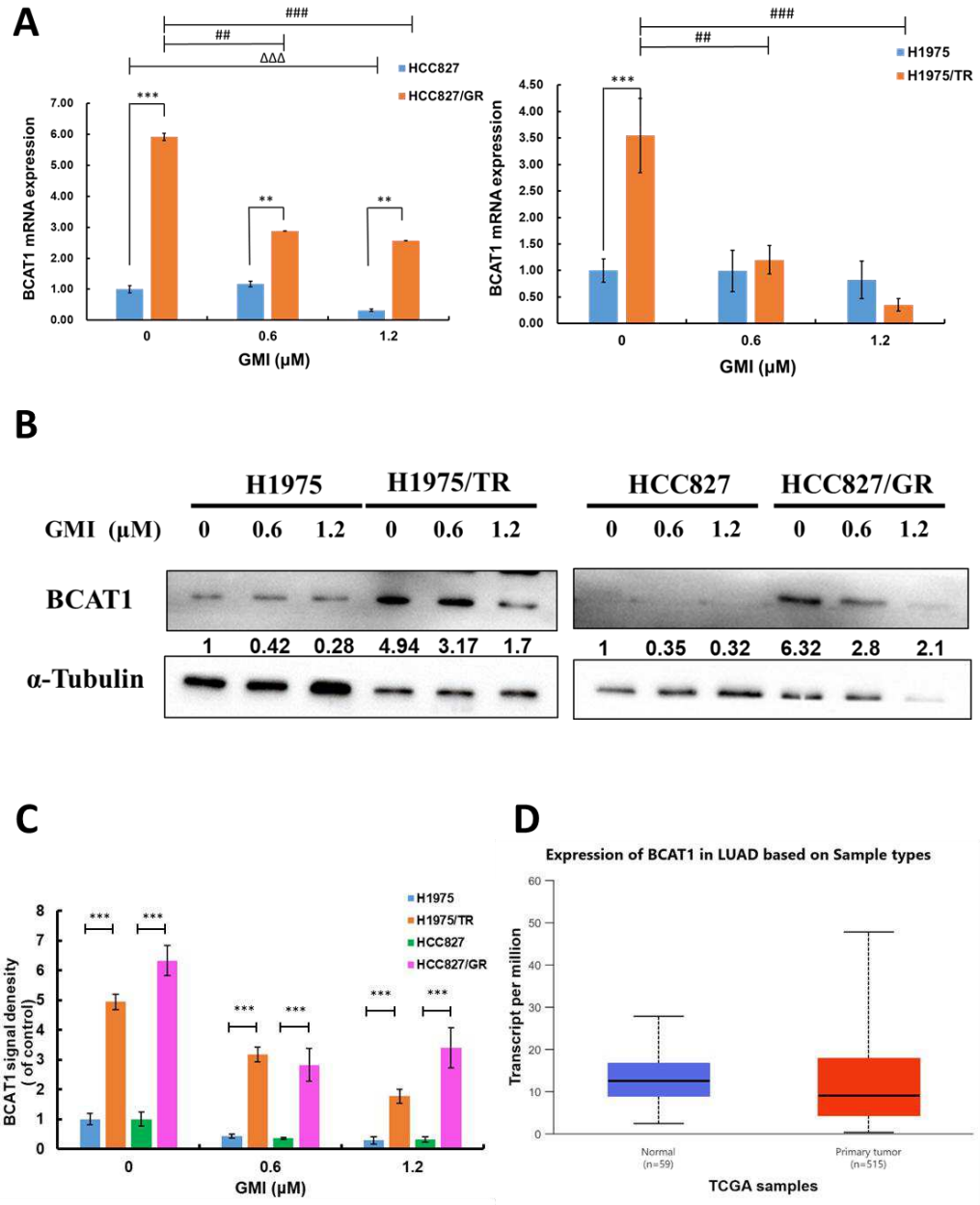
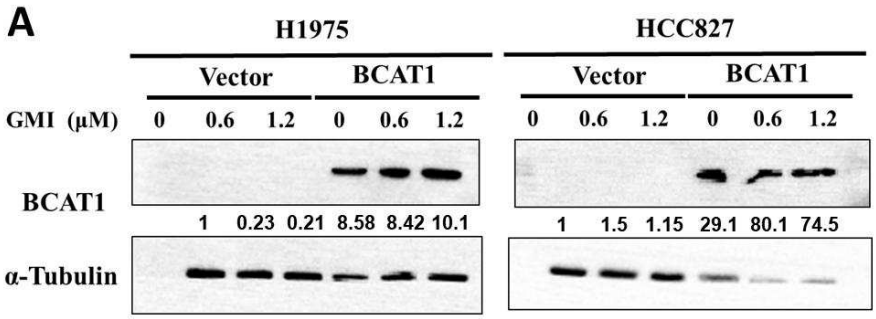


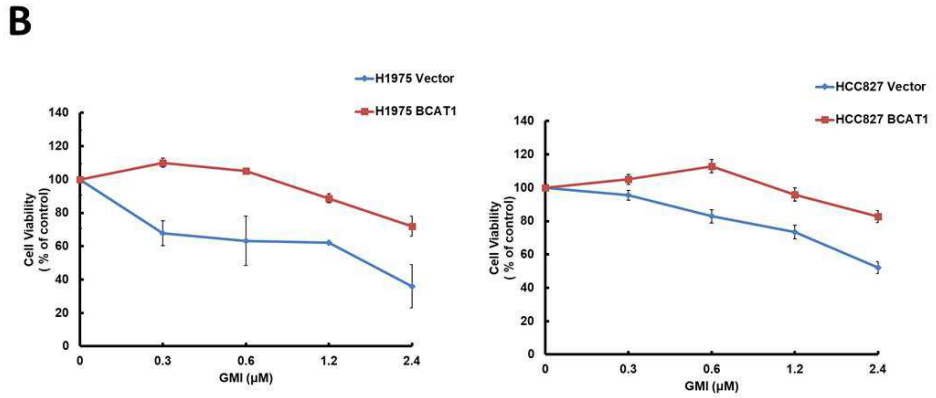
Figure 2. GMI downregulates BCAT1 expression in EGFR-TKI-resistant NSCLC cells.

(A) Quantitative analysis of BCAT1 mRNA expression in parental HCC827 and H1975 cells and their corresponding gefitinib- and osimertinib-resistant sublines (HCC827/GR and H1975/TR, respectively) following treatment with GMI (0, 0.6, or 1.2 μM). BCAT1 mRNA expression was evaluated by quantitative real-time PCR (qRT-PCR). (B) Representative Western blot analysis of BCAT1 protein expression in H1975, H1975/TR, HCC827, and HCC827/GR cells treated with different concentrations of

GMI (0, 0.6, or 1.2 μM). α-Tubulin was used as the internal loading control. The relative expression levels of BCAT1 are indicated below the corresponding bands. (C) Densitometric quantification of BCAT1 protein expression shown in (B). BCAT1 protein levels were normalized to the corresponding loading controls and expressed relative to the untreated parental cell control. (D) Analysis of BCAT1 mRNA expression in normal lung tissues (n = 59) and primary lung adenocarcinoma (LUAD) tissues (n = 515) using The Cancer Genome Atlas (TCGA) dataset.Data are presented as the mean ± SD. Statistical significance was determined using the appropriate statistical tests. P < 0.01, *P < 0.001; ##P < 0.01, ###P < 0.001.

Figure 3


A
H1975
HCC827
Vector
BCAT1
Vector
BCAT1
GMI (μM)
0 0.6 1.2 0 0.6 1.2
0 0.6 1.2 0 0.6 1.2
BCAT1
1 0.23 0.21 8.58 8.42 10.1
1 1.5 1.15 29.1 80.1 74.5
α-Tubulin


B
H1975 Vector
H1975 BCAT1
Cell Viability (% of control)
GMI (μM)
HCC827 Vector
HCC827 BCAT1
Cell Viability (% of control)
GMI (μM)

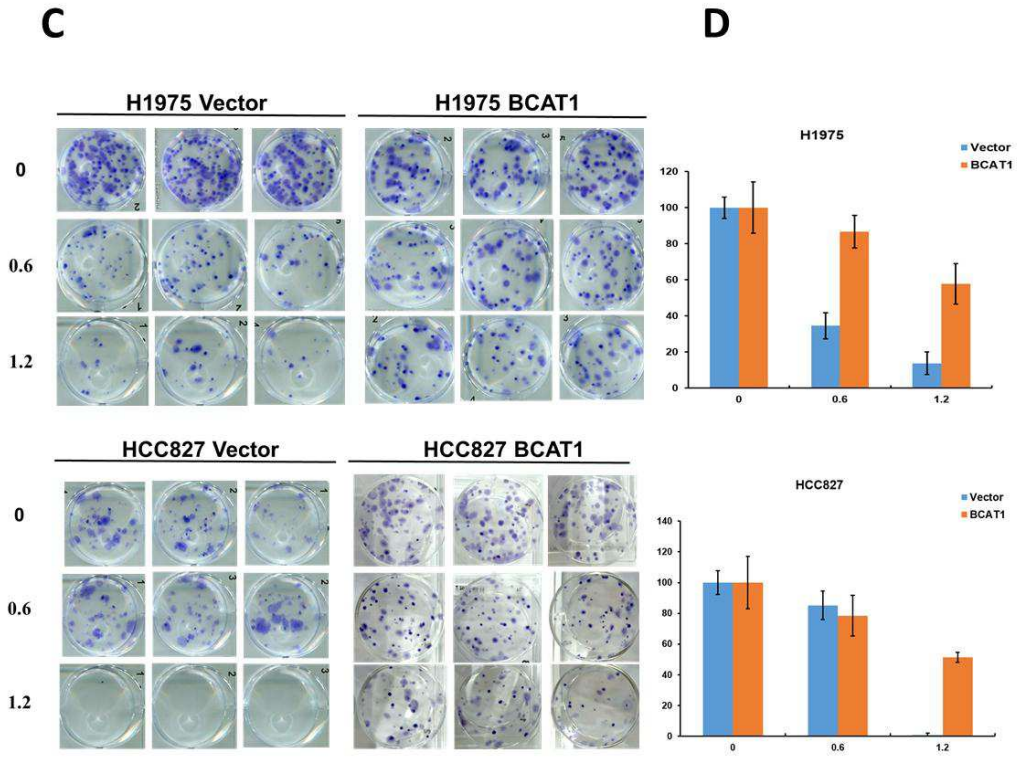

C
H1975 Vector
H1975 BCAT1
0
0.6
1.2
HCC827 Vector
HCC827 BCAT1
0
0.6
1.2
D
H1975
Vector
BCAT1
HCC827
Vector
BCAT1

Figure 3. BCAT1 overexpression attenuates the inhibitory effects of GMI on EGFR-TKI-resistant NSCLC cell viability and colony formation.

(A) Western blot analysis confirming BCAT1 overexpression in H1975 and HCC827 cells transfected with a BCAT1 expression vector or an empty vector (Vector). Cells were treated with GMI at the indicated concentrations (0, 0.6, and 1.2 μM). α-Tubulin was used as the loading control. The relative BCAT1 protein expression levels are indicated below the corresponding bands. (B) Cell viability analysis of H1975 and HCC827 cells transfected with either the empty vector or BCAT1 expression vector following treatment with GMI at the indicated concentrations (0, 0.3, 0.6, 1.2, and 2.4 μM). Cell viability was determined using the MTT assay and expressed as a percentage of the untreated control. (C) Representative images of colony formation assays in H1975 and HCC827 cells transfected with the empty vector or BCAT1 expression vector and treated with GMI (0, 0.6, and 1.2 μM). Cells were cultured for 10–14 days, followed by crystal violet staining to visualize colony formation. (D) Quantitative analysis of colony formation shown in (C), illustrating the effects of BCAT1 overexpression on GMI-mediated suppression of clonogenic growth in H1975 and HCC827 cells. Data are presented as the mean ± SD from three independent experiments.

Figure 4

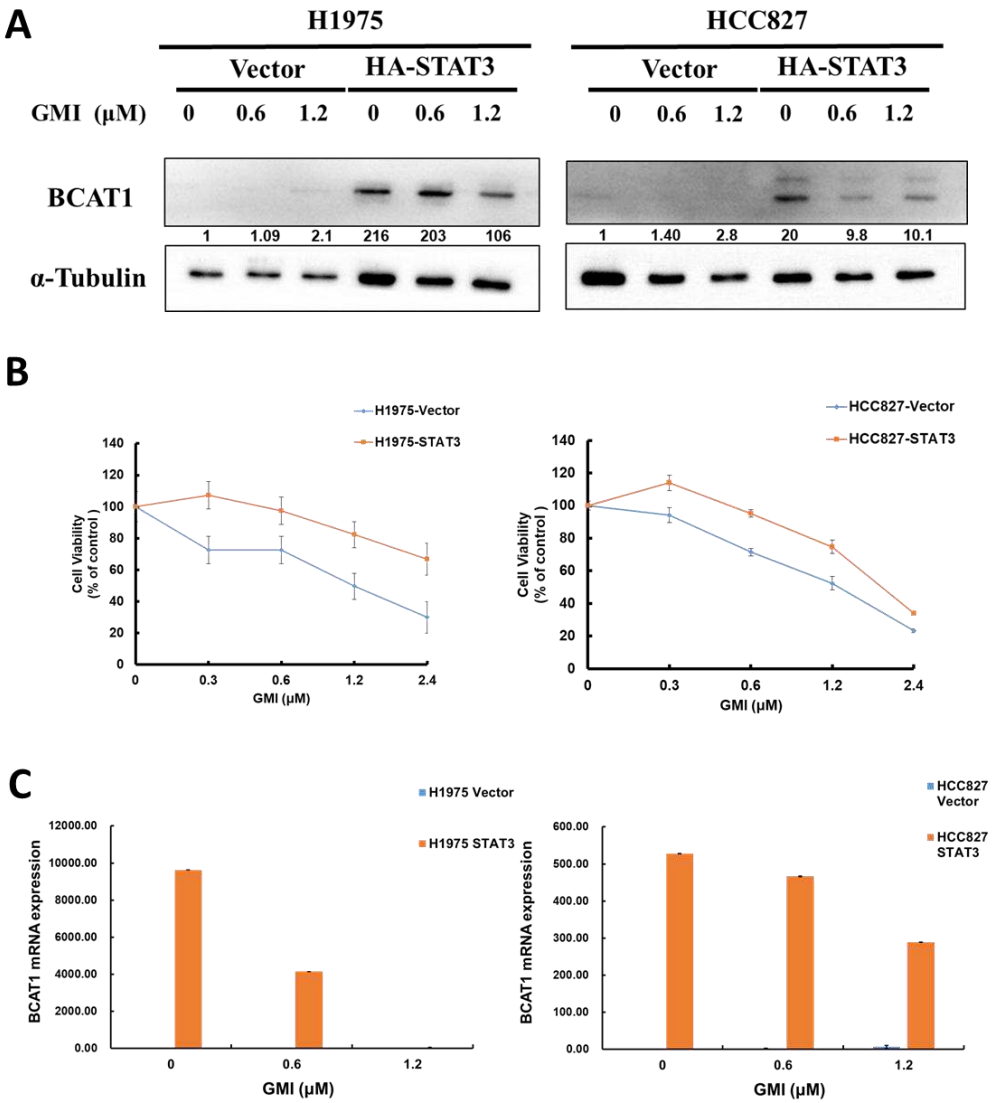


Figure 4. STAT3 overexpression enhances BCAT1 expression and attenuates the inhibitory effects of GMI on lung cancer cell viability.

(A) H1975 and HCC827 cells transfected with empty vector or HA-tagged STAT3 (HA-STAT3) were treated with GMI (0, 0.6, and 1.2 μM). BCAT1 protein expression was evaluated by Western blotting, with α-tubulin serving as the internal loading control. The relative protein expression levels of BCAT1 were quantified and normalized to the corresponding control groups. (B) Cell viability of H1975 and HCC827 cells transfected with empty vector or HA-STAT3 following treatment with GMI at the indicated concentrations (0, 0.3, 0.6, 1.2, and 2.4 μM). Cell viability was determined and expressed as a percentage of the untreated control. (C) Quantitative real-time PCR analysis of BCAT1 mRNA expression in H1975 and HCC827 cells transfected with empty vector or HA-STAT3 following treatment with GMI (0, 0.6, and 1.2 μM). BCAT1

mRNA expression was normalized to the internal reference gene and expressed relative to the corresponding control group. Data are presented as mean ± SD.

Figure 5

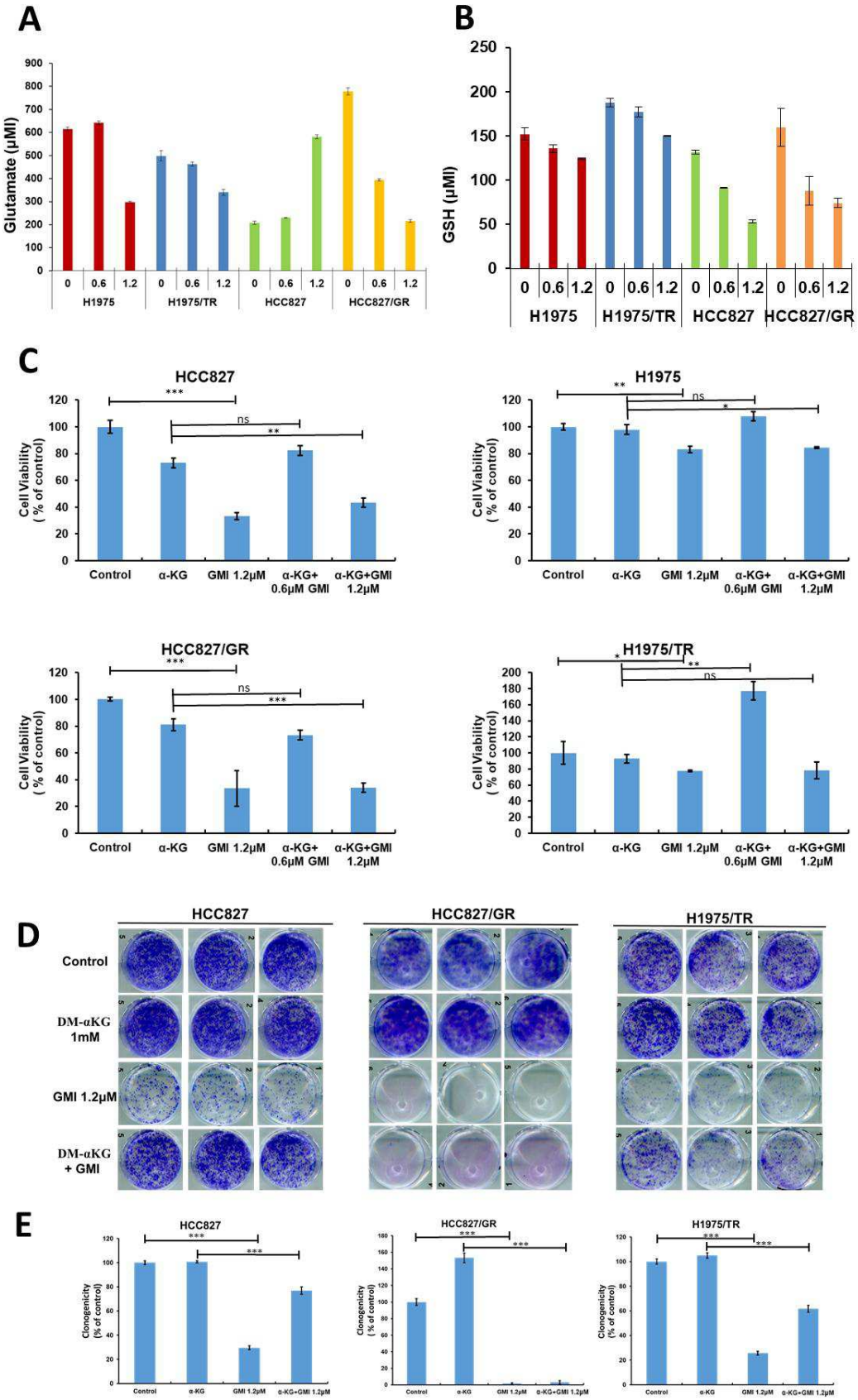

A
Glutamate (μMl)
900
800
700
600
500
400
300
200
100
0
0 0.6 1.2 0 0.6 1.2 0 0.6 1.2 0 0.6 1.2
H1975
H1975/TR
HCC827
HCC827/GR
B
GSH (μMl)
250
200
150
100
50
0
0 0.6 1.2 0 0.6 1.2 0 0.6 1.2 0 0.6 1.2
H1975
H1975/TR
HCC827
HCC827/GR
C
HCC827
Cell Viability (% of control)
***
ns
**
Control
α-KG
GMI 1.2μM
α-KG+ 0.6μM GMI
α-KG+GMI 1.2μM
H1975
**
ns
*
HCC827/GR
***
ns
***
H1975/TR
*
**
ns
D
HCC827
HCC827/GR
H1975/TR
Control
DM-αKG 1mM
GMI 1.2μM
DM-αKG + GMI
E
HCC827
HCC827/GR
H1975/TR
Clonogenicity (% of control)
***
Control
α-KG
GMI 1.2μM
α-KG+GMI 1.2μM

Figure 5. GMI regulates glutamate metabolism and glutathione levels, while α-ketoglutarate supplementation modulates GMI-induced suppression of lung cancer cell viability and clonogenic survival.

(A) Intracellular glutamate levels in H1975, H1975/TR, HCC827, and HCC827/GR cells following treatment with GMI (0, 0.6, and 1.2 μM). Glutamate concentrations were measured and expressed in μM. (B) Intracellular glutathione (GSH) levels in H1975, H1975/TR, HCC827, and HCC827/GR cells following treatment with GMI (0, 0.6, and 1.2 μM). GSH concentrations were measured and expressed in μM. (C) Effects of dimethyl α-ketoglutarate (DM-αKG) supplementation on cell viability in HCC827, H1975, HCC827/GR, and H1975/TR cells following GMI treatment. Cells were treated with DM-αKG (1 mM), GMI (1.2 μM), or a combination of DM-αKG (1 mM) and GMI (0.6 or 1.2 μM), as indicated. Cell viability was determined and expressed as a percentage of the untreated control. (D) Representative images of colony formation assays in HCC827, HCC827/GR, and H1975/TR cells treated with DM-αKG (1 mM), GMI (1.2 μM), or their combination. Cells were stained with crystal violet to evaluate clonogenic survival. (E) Quantification of clonogenic survival in HCC827, HCC827/GR, and H1975/TR cells following the indicated treatments. Colony-forming ability was quantified, normalized to the untreated control, and expressed as a percentage. Data are presented as mean ± SD. Statistical significance is indicated as follows: $P < 0.05$, $P < 0.01$, and $P < 0.001$; ns, not significant.

Figure 6

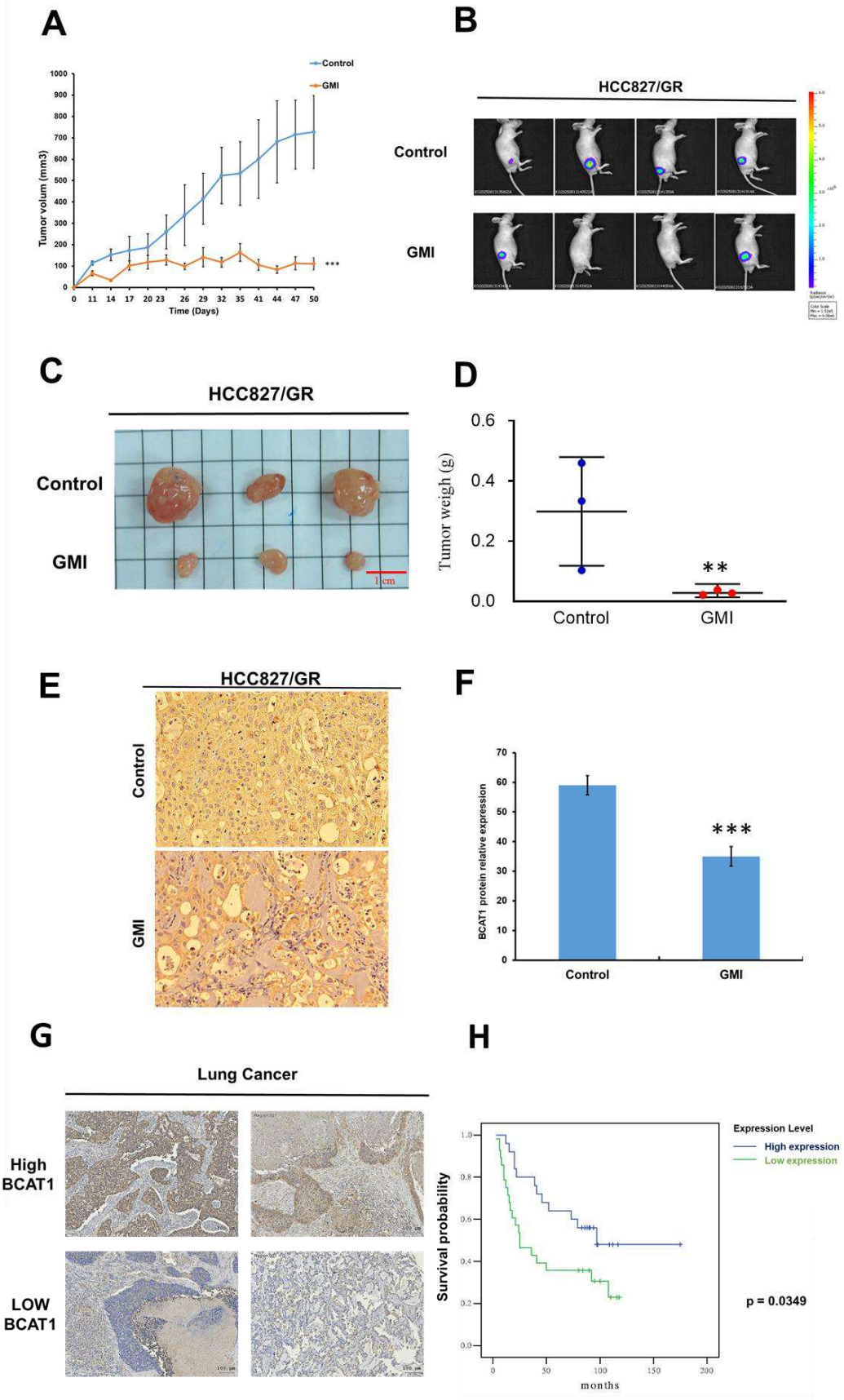

A
Control
GMI
Tumor volum (mm3)
Time (Days)
***
B
HCC827/GR
Control
GMI
C
HCC827/GR
Control
GMI
1 cm
D
Tumor weigh (g)
**
Control
GMI
E
HCC827/GR
Control
GMI
F
BCAT1 protein relative expression
***
Control
GMI
G
Lung Cancer
High BCAT1
LOW BCAT1
H
Survival probability
months
Expression Level
High expression
Low expression
p = 0.0349

Figure 6. GMI suppresses the growth of HCC827/GR xenograft tumors and reduces BCAT1 expression in vivo, while high BCAT1 expression is associated with poor survival in patients with lung cancer.

(A) Tumor growth curves of mice bearing HCC827/GR xenografts treated with vehicle (Control) or GMI. Tumor volumes were measured at the indicated time points throughout the treatment period. (B) Representative bioluminescence images of mice bearing HCC827/GR xenografts in the control and GMI-treated groups at the end of the experimental period. (C) Representative images of excised HCC827/GR xenograft tumors collected from the control and GMI-treated groups. (D) Comparison of tumor weights between the control and GMI-treated groups. Individual data points represent tumor weights from individual mice. (E) Representative immunohistochemical staining images showing BCAT1 expression in HCC827/GR xenograft tumor tissues obtained from the control and GMI-treated groups. (F) Quantification of BCAT1 protein expression in xenograft tumor tissues from the control and GMI-treated groups. Relative BCAT1 expression was quantified based on immunohistochemical staining. (G) Representative immunohistochemical images of human lung cancer tissues showing high and low BCAT1 expression. (H) Kaplan–Meier survival analysis of patients with lung cancer stratified according to high or low BCAT1 expression. Patients with high BCAT1 expression exhibited significantly poorer overall survival than those with low BCAT1 expression ($P = 0.0349$). Data are presented as mean ± SD, where applicable. Statistical significance is indicated as follows: $^{**}P < 0.01$ and $^{***}P < 0.001$.

Supplementary Files

This is a list of supplementary files associated with this preprint. Click to download.

- RAWDATA.pdf